

Thermal Pure States for Systems with Antiunitary Symmetries and Their Tensor Network Representations

Yasushi Yoneta^{1,*}

¹ Center for Quantum Computing, RIKEN, 2-1 Hirosawa, Wako, Saitama 351-0198, Japan

(Dated: December 18, 2024)

Thermal pure state algorithms, which employ pure quantum states representing thermal equilibrium states instead of statistical ensembles, are useful both for numerical simulations and for theoretical analysis of thermal states. However, their inherently large entanglement makes it difficult to represent efficiently and limits their use in analyzing large systems. Here, we propose a new tensor network algorithm for constructing thermal pure states for systems with certain antiunitary symmetries, such as time-reversal or complex conjugate symmetry. Our method utilizes thermal pure states that, while exhibiting volume-law entanglement, can be mapped to tensor network states through simple transformations. Furthermore, our approach does not rely on random sampling and thus avoids statistical uncertainty. Moreover, we can compute not only thermal expectation values of local observables but also thermodynamic quantities. We demonstrate the validity and utility of our method by applying it to the one-dimensional XY model and the two-dimensional Ising model on a triangular lattice. Our results suggest a new class of variational wave functions for volume-law states that are not limited to thermal equilibrium states.

Introduction— Formulating statistical mechanics using pure states has attracted significant attention across various fields, from quantum statistical physics [1–6] to quantum gravity [7–10]. This approach employs thermal pure states, which are locally indistinguishable from thermal equilibrium states, instead of statistical ensembles, to derive the thermal properties. Thermal pure states are utilized not only for finite-temperature simulations [11–25] but also for theoretical analysis to gain deep insights into the structure of thermal equilibrium states [26–28].

The seminal works by Sugiura and Shimizu [4, 5] provided a method for constructing thermal pure states, called the TPQ states, using Haar random states. They proved that the TPQ states yield thermal expectation values and thermodynamic quantities with an exponentially small probability of error in the thermodynamic limit. However, the complexity of Haar random states makes it difficult to represent efficiently, and numerical simulations are limited to systems of 30–40 sites. Furthermore, statistical-mechanical quantities computed from the TPQ states have uncertainties due to their randomness, which become more pronounced at lower temperatures where the number of states decreases.

Thermal pure states must have a large amount of entanglement obeying a volume law because they are locally indistinguishable from the Gibbs state, whose von Neumann entropy of the reduced density matrix is equal to the thermodynamic entropy. This presents a major challenge in efficiently representing thermal pure states using variational wave functions. This is because tensor network states, such as matrix product states (MPS) [29–33], which are the most widely used variational wave functions for quantum many-body states, require a small amount of entanglement to be represented with a small number of parameters. Thus, algorithms such as the METTS method [34, 35] and the TPQ-MPS method [36–

38], which cleverly decompose the statistical ensemble into a convex mixture of low-entanglement pure states, are also employed in practical applications. However, to accurately recover the properties of the original ensemble, one needs to repeat the sampling of these states to reduce statistical uncertainties [39].

In developing efficient algorithms, it is crucial to leverage symmetries. While unitary symmetries are often the primary focus, many realistic quantum many-body systems also possess antiunitary symmetries, such as time-reversal symmetry. It is known that antiunitary symmetries play a significant role in the study of quantum chaos [40]. Given their importance, it is an intriguing question whether finite-temperature simulations can be fast-forwarded under such symmetries.

In a previous paper [41], the authors proposed a new type of thermal pure states, constructed in a manner quite different from existing thermal pure states. These states are obtained from well-structured states, termed entangled antipodal pair (EAP) states, rather than Haar random states. However, the structured nature of the EAP states was not fully exploited, restricting their numerical application to small systems. Furthermore, their applicability was limited to one-dimensional systems with complex conjugate symmetry.

The main contribution of this paper is to develop an efficient tensor network algorithm for constructing thermal pure states derived from EAP states, addressing the limitations of existing finite-temperature pure state algorithms in practical applications. To this end, we focus on the well-structured and deterministic natures of the EAP state, which facilitates the efficient construction and representation of the derived states and frees them from statistical uncertainty. First, we generalize the EAP states to make our algorithm applicable to systems other than one-dimensional systems with complex conjugate

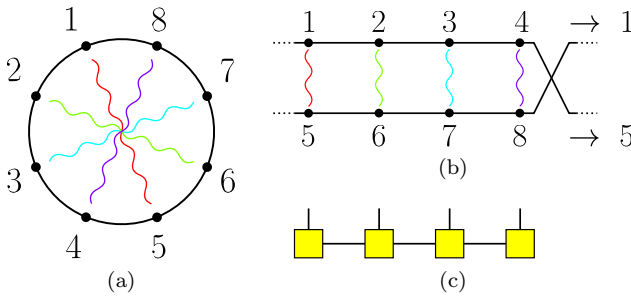


FIG. 1. (a) Schematic diagram depicting an entangled antipodal pair state $|\text{EAP}(\hat{u})\rangle$ for a one-dimensional system with periodic boundary conditions. Wavy lines represent the maximally entangled states $|\Phi(\hat{u})\rangle$. (b) A system on a ring can be mapped to one on a ladder with Möbius boundary conditions while preserving the short-range nature of the interactions. In this correspondence, the EAP state is mapped to a state with only local entanglement. (c) Therefore, it can be represented as an MPS with a local dimension 4 and a bond dimension 1.

symmetry. Next, we present thermal pure states constructed from these EAP states and provide formulas for statistical-mechanical quantities using these states. Furthermore, we develop a tensor network algorithm for efficiently constructing these states. Finally, we demonstrate the validity and usefulness of our method by applying it to paradigmatic models in one and two dimensions.

EAP state— We consider a closed quantum system composed of spins on a d -dimensional lattice $\Lambda = \prod_{i=1}^d \{1, 2, \dots, L_i\}$ with periodic boundary conditions. We write the system size as $N = \prod_{i=1}^d L_i$. We assume that the side length L_1 in the first direction is even. Let $d(r, r')$ denote the distance between two points $r, r' \in \Lambda$ on the lattice. Let $\hat{\sigma}^\mu (\mu = x, y, z)$ be the Pauli matrices, and $|0\rangle$ and $|1\rangle$ be the eigenvectors of $\hat{\sigma}^z$. We call the basis of the whole Hilbert space formed by the tensor products of $|0\rangle$ and $|1\rangle$ the spin basis.

As for the preparation, we define the antipodal site for each lattice site. Let the mapping p that assigns each lattice site $r \in \Lambda$ to its antipodal site $p(r) \in \Lambda$. In this paper, we select the simplest choice as [42]

$$p(r_1, r_2, \dots, r_d) = (r_1 + L_1/2 \bmod L_1, r_2, \dots, r_d). \quad (1)$$

With this choice, $p(r)$ corresponds to the antipodal point of r on the “meridian” of the d -dimensional torus. We can divide the lattice Λ into the “left half”, denoted as Λ_L , and its complement, ensuring that each subsystem contains exactly one site from each antipodal pair. Specifically, Λ_L is defined as

$$\Lambda_L = \{(r_1, r_2, \dots, r_d) \in \Lambda \mid 1 \leq r_1 \leq L_1/2\}. \quad (2)$$

Now, we define the EAP state for the spin-1/2 system on Λ [43]. Let \hat{u} be a 2×2 unitary matrix that is either symmetric or antisymmetric,

$$\hat{u}^T \equiv (-1)^k \hat{u} \quad (k \in \mathbb{Z}), \quad (3)$$

where the superscript T denotes the transpose in the $\{|0\rangle, |1\rangle\}$ basis. As explained below Eq. (7), \hat{u} is chosen according to the antiunitary symmetry of the system. Then we define the EAP state associated with \hat{u} as [44]

$$|\text{EAP}(\hat{u})\rangle = \bigotimes_{r \in \Lambda_L} |\Phi(\hat{u})\rangle_{r,p(r)}. \quad (4)$$

Here $|\Phi(\hat{u})\rangle_{r,p(r)}$ is a maximally entangled state between antipodal pairs of spins at sites r and $p(r)$ defined by [45]

$$|\Phi(\hat{u})\rangle_{r,p(r)} = \hat{I} \otimes \hat{u} \left[|0\rangle_r |0\rangle_{p(r)} + |1\rangle_r |1\rangle_{p(r)} \right], \quad (5)$$

where \hat{I} and \hat{u} act on site r and $p(r)$, respectively. Although this state might appear to be macroscopically inhomogeneous, it is invariant under translations (up to the sign) because $|\Phi(\hat{u})\rangle_{r,p(r)}$ is (anti)symmetric under the exchange of r and $p(r)$, i.e., $\text{Swap}_{r,p(r)}|\Phi(\hat{u})\rangle_{r,p(r)} = (-1)^k |\Phi(\hat{u})\rangle_{r,p(r)}$.

One remarkable property of the EAP state is that it is locally indistinguishable from the Gibbs state

$$\hat{\rho}_N^{\text{can}}(\beta) = \frac{e^{-\beta \hat{H}}}{Z} \quad (6)$$

at the inverse temperature $\beta = 0$ [41]. Here $Z = \text{Tr}[e^{-\beta \hat{H}}]$ is a partition function. In fact, the reduced density matrix of the EAP state for any subsystem $X (\subset \Lambda)$ with diameter $D(X) = \max_{r,r' \in X} d(r, r')$ less than $L_1/2$ coincides with the maximally mixed state $\propto \hat{I}_X$, which equals that for the Gibbs state at $\beta = 0$. Thus, EAP states are thermal pure states at infinite temperature. In the following, we present a method to construct thermal pure states at finite temperatures from EAP states.

Imaginary-time evolved EAP state— We can generate a finite-temperature thermal pure state from an EAP state. In doing so, the EAP state must be chosen appropriately according to the symmetry of the system.

Consider a system with translation-invariant short-range interactions. We assume that the Hamiltonian \hat{H} is invariant

$$\hat{\Theta}^\dagger \hat{H} \hat{\Theta} = \hat{H} \quad (7)$$

under an antiunitary transformation expressed as $\hat{\Theta} = \hat{u}^{\otimes N} \hat{K}$, where \hat{u} is a 2×2 unitary matrix satisfying $\hat{u}^T = (-1)^k \hat{u}$, and \hat{K} represents the complex conjugation with respect to the spin basis. Hamiltonians satisfying Eq. (7) can be classified into following two classes:

1. Hamiltonians whose matrix representations with respect to the spin basis are real, $\hat{H} = \hat{H}_{\text{real}}$ (the case of $\hat{u} = \hat{I}$), and their conjugations by global SU(2) spin rotations $\hat{W} = \hat{w}^{\otimes N}$, $\hat{H} = \hat{W}^\dagger \hat{H}_{\text{real}} \hat{W}$ (the case of $\hat{u} = \hat{w}\hat{w}^T$),
2. Hamiltonians with time-reversal symmetry (the case of $\hat{u} = i\hat{\sigma}^y$).

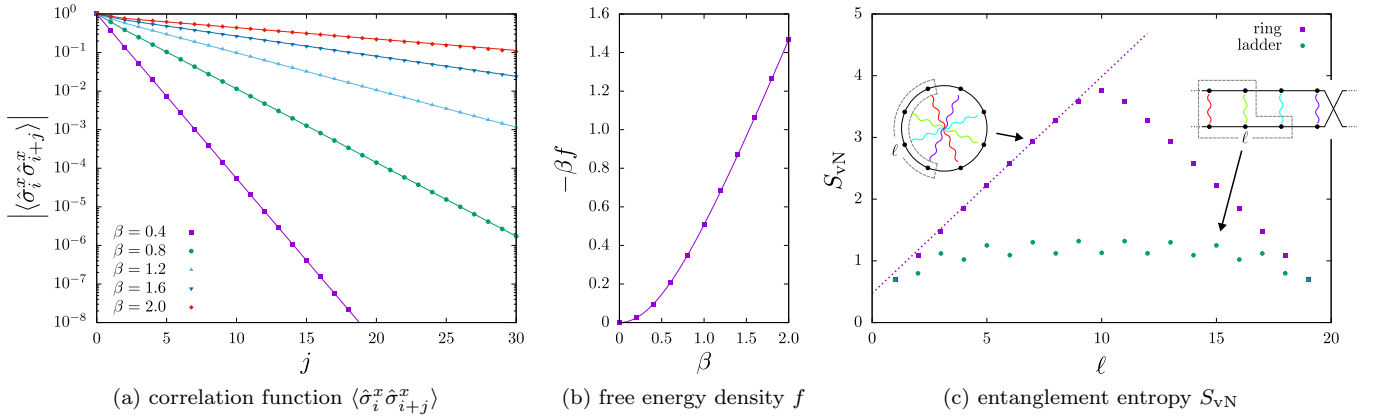


FIG. 2. Properties of the ITE-EAP state for the one-dimensional XY model with $J^{xx} = 1$, $J^{yy} = 1/2$. (a) Two-point correlation function $\langle \hat{o}_i^x \hat{o}_{i+j}^x \rangle$ and (b) free energy density f for a 200-site chain. The solid lines represent the exact values in the thermodynamic limit. (c) Entanglement entropy for a 20-site chain at the inverse temperature $\beta = 1$ as a function of subsystem size ℓ . The system is partitioned in two different ways: (purple squares) by cutting the original ring and (green circles) by cutting the ladder obtained by rearrangement. The dotted line represents the volume law whose coefficients corresponds to the exact value of the thermodynamic entropy density at the same temperature. Imaginary-time evolution is carried out using a second-order Trotter decomposition with an imaginary time step of 0.05 and a truncation threshold of 10^{-14} .

These classes include various models of interest in statistical mechanics.

We define the imaginary-time evolved EAP (ITE-EAP) state at the inverse temperature β as an unnormalized state obtained by evolving the EAP state associated with \hat{u} in imaginary time $\beta/4$:

$$|\beta\rangle = e^{-\frac{1}{4}\beta\hat{H}} |\text{EAP}(\hat{u})\rangle. \quad (8)$$

Then, for any local observable \hat{O} , this state is indistinguishable from the Gibbs state $\hat{\rho}_N^{\text{can}}(\beta)$ at the same inverse temperature β [46]:

$$\lim_{N \rightarrow \infty} \text{Tr} \left[\hat{\rho}_N^{\text{can}}(\beta) \hat{O} \right] = \lim_{N \rightarrow \infty} \frac{\langle \beta | \hat{O} | \beta \rangle}{\langle \beta | \beta \rangle}. \quad (9)$$

In other words, $|\beta\rangle$ is a thermal pure state at the inverse temperature β .

Moreover, one can also calculate the free energy density f from the norm of the ITE-EAP state as [46]

$$-\beta f(\beta) = \lim_{N \rightarrow \infty} \frac{1}{N} \log Z = \lim_{N \rightarrow \infty} \frac{2}{N} \log \langle \beta | \beta \rangle. \quad (10)$$

Therefore, one can obtain all thermodynamic quantities, including the thermodynamic entropy and specific heat, as these quantities can be computed from the free energy [47].

Here, we should mention the distinction between the ITE-EAP state and a purified Gibbs state [48, 49]. The purified Gibbs state is a pure state of an extended system that includes an ancillary system, and when focusing only on the target system, it is completely identical to the Gibbs state in all physical properties. As the Gibbs state is characterized as the state that maximizes the

von Neumann entropy [50, 51], it is a highly mixed state. Therefore, it cannot be used to analyze properties unique to pure states. In contrast, the ITE-EAP state is a pure state of a closed system and thus serves as a theoretical example of a pure state in thermal equilibrium, providing access to properties of such a state, including the entanglement structure [26, 27].

Tensor network method— As discussed in the introduction, thermal pure states generally exhibit volume-law entanglement and therefore cannot be efficiently represented as tensor network states. However, ITE-EAP states, despite also obeying a volume law, can be brought into forms that can be efficiently represented as tensor network states through simple transformations due to the well-structured nature of EAP states. This makes them useful for numerical calculations.

Let us describe a tensor network method for constructing the ITE-EAP state, taking an example of a one-dimensional system $\Lambda = \{1, 2, \dots, N\}$ (Fig. 1a). Apparently, the EAP state contains a large amount of long-range entanglement between sites separated by $N/2$ (Fig. 1a). To address this, we map the ring to a ladder of length $N/2$ (Fig. 1b):

$$\Lambda \ni j \mapsto \begin{cases} [A, j] & (j \leq N/2) \\ [B, j - N/2] & (\text{otherwise}) \end{cases}, \quad (11)$$

where $[A, j]$ and $[B, j]$ denote the j -th site on the upper and lower chains of the ladder, respectively [52, 53]. Here, to ensure that the system is mapped to a translation-invariant and short-range interacting system on the ladder, we adopt Möbius boundary conditions:

$$[A, N/2 + 1] = [B, 1], \quad [B, N/2 + 1] = [A, 1]. \quad (12)$$

Then the antipodal pair (j and $p(j) = j + N/2$) on the ring maps to a pair of spins ($[A, j]$ and $[B, j]$) aligned vertically on the ladder, so the maximally entangled state $|\Phi(\hat{u})\rangle_{j,p(j)}$ is local on the ladder. Thus, by treating the vertically aligned pair of spins as a single site $\cong \mathbb{C}^4$, the EAP state can be regarded as a product state without any spatial entanglement and can be represented as an MPS with a bond dimension 1 (Fig. 1c). Consequently, the ITE-EAP state, which is the imaginary-time evolution of this state with a Hamiltonian where the interactions are short ranged (except for boundary terms introduced to impose the Möbius boundary conditions [54]), is expected to contain only a small amount of entanglement and can be efficiently represented as an MPS, as demonstrated in the example below. Thus, by performing the imaginary-time evolution with a small time step $\delta\beta/4$ using the time-evolving block decimation algorithm [48, 55–57], one can efficiently obtain a series of ITE-EAP states at the inverse temperatures $0, \delta\beta, 2\delta\beta, \dots$.

Application 1: one-dimensional XY model— To demonstrate the validity and utility of the ITE-EAP state, we apply our method to the one-dimensional XY model, whose exact solutions are known [58], defined by the Hamiltonian

$$\hat{H} = \sum_{j=1}^N [J^{xx} \hat{\sigma}_j^x \hat{\sigma}_{j+1}^x + J^{yy} \hat{\sigma}_j^y \hat{\sigma}_{j+1}^y]. \quad (13)$$

Since this Hamiltonian has time-reversal symmetry, we can choose $\hat{u} = i\hat{\sigma}^y$ to satisfy Eq. (7) and generate the ITE-EAP state from the EAP associated with this \hat{u} [59]. Following the algorithm explained above, we successfully constructed the ITE-EAP state for $N = 200$, a significant improvement compared to the TPQ algorithm, which is limited to about 30 sites.

Figure 2a shows the two-point correlation function $\langle \hat{\sigma}_i^x \hat{\sigma}_{i+j}^x \rangle$ calculated using the ITE-EAP state. The results are in good agreement with the exact solution in the thermodynamic limit, confirming that the ITE-EAP state is a thermal pure state (and, of course, free from statistical uncertainty). Furthermore, as shown in Figure 2b, the free energy calculated using the ITE-EAP state also agrees with the exact value.

We also investigate the entanglement properties of the ITE-EAP state. Figure 2c shows the entanglement profile of the ITE-EAP state when the system is partitioned in two different ways. When the system is divided into two subsystems by cutting the original ring, the entanglement entropy between them obeys a volume law. Moreover, it can be seen that the coefficient of the volume law agrees with the thermodynamic entropy density. This not only corroborates the ITE-EAP state as a thermal pure state but also enables us to extract the thermodynamic entropy from the entanglement scaling. In contrast, when the system is divided by cutting the ladder after rearrangement, the entanglement entropy obeys an area law.

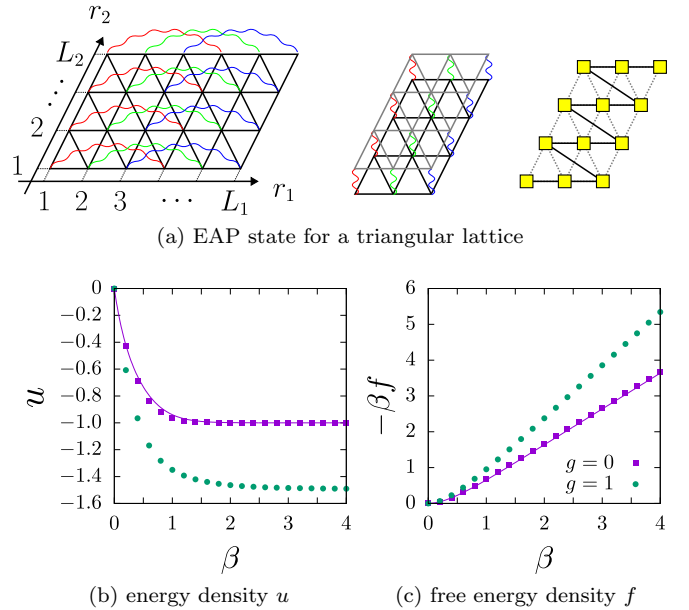


FIG. 3. (a) Schematic diagram depicting the triangular lattice and the EAP state employed in our numerical calculations. Wavy lines represent the maximally entangled state. (b) Energy density $u = \langle \hat{H} \rangle / N$ and (c) free energy density f obtained from the ITE-EAP state for the two-dimensional transverse-field Ising model on the triangular lattice with $J = 1$, $L_1 = 6$, and $L_2 = 10$. Imaginary-time evolution is carried out using a second-order Trotter decomposition with an imaginary time step of 0.05 and a truncation threshold of 10^{-8} .

This enables the efficient representation of the ITE-EAP state as an MPS and dealing with large systems.

Application 2: two-dimensional Ising model on a triangular lattice— Our algorithm can be directly generalized to two-dimensional systems. Let us apply the ITE-EAP state to the antiferromagnetic transverse-field Ising model on a triangular lattice of size $N = L_1 \times L_2$ with periodic boundary conditions (left of Fig. 3a). The Hamiltonian is given by

$$\hat{H} = J \sum_{\langle r, r' \rangle} \hat{\sigma}_r^z \hat{\sigma}_{r'}^z - g \sum_r \hat{\sigma}_r^x \quad (J > 0), \quad (14)$$

where $\langle r, r' \rangle$ denotes the nearest-neighbor pairs. This model reduces to the classical Ising model as $g \rightarrow 0$, whose exact results at finite temperature have been derived for $N \rightarrow \infty$ [60]. Since this Hamiltonian is real in the spin basis, choosing $\hat{u} = \hat{I}$ satisfies Eq. (7). Then, using this \hat{u} , we define the EAP state and construct the ITE-EAP state. In numerical calculations, similar to the one-dimensional case, we fold the lattice so that the antipodal sites are adjacent to each other (center of Fig. 3a) and represent the EAP and ITE-EAP states as a snake MPS on the folded lattice (right of Fig. 3a).

Figures 3b and 3c show the β -dependence of the energy density and free energy calculated from the ITE-EAP state, respectively. Firstly, in the case of $g = 0$,

it is confirmed that the results for the ITE-EAP state agree with the exact values. Additionally, numerical calculations are also feasible for $g = 1$, successfully reaching 60 sites. If we were to keep the state vector in a brute-force way, similar to the TPQ algorithm, it would require an enormous amount of memory, on the order of 10^7 TB. However, due to the well-structured nature of the EAP state underlying the ITE-EAP state, it is possible to investigate the thermal properties of large systems using only about 10^0 GB of memory.

Conclusion— We have extended the method of constructing finite-temperature thermal pure states based on EAP states, originally provided only for one-dimensional systems with complex conjugate symmetry, to systems with time-reversal symmetry or complex conjugate symmetry on general lattices. Using these states, we can calculate not only thermal expectation values of local observables but also thermodynamic quantities. Furthermore, we have developed an efficient numerical method using tensor networks for these states. Our algorithm allows for a much more efficient representation on a classical computer compared to the TPQ algorithm. In addition, since our algorithm does not rely on random sampling, it does not suffer from statistical uncertainty and enables us to calculate all statistical-mechanical quantities accurately only from a single state. We have demonstrated the validity and utility of our method by applying it to the one-dimensional XY model and the two-dimensional Ising model on a triangular lattice.

There are several directions for future work. First, it is an important task to extend the applicability of our algorithm, which is currently restricted to systems with certain types of antiunitary symmetries. Second, developing an efficient algorithms for finite-temperature nonequilibrium simulations using the ITE-EAP state is also an important challenge. While the ITE-EAP state can correctly describe dynamics starting from an equilibrium state, as time evolves, it loses its simple entanglement structure, making it difficult for naive methods to access long timescales [46]. Third, our results suggest the high expressivity of states obtained by applying matrix product operators to EAP states. This implies the potential to use these states as variational wave functions for a broader class of volume-law states beyond thermal pure states. Therefore, investigating the expressivity of states derived from EAP states is also an interesting challenge. Finally, EAP states could be applied to quantum algorithms. This is because EAP states can be easily constructed using single-depth quantum circuits with local two-qubit gates by rearranging qubits similarly to the algorithm presented in this paper. This contrasts with the Haar random state, which is hard to construct [61–63].

Acknowledgments— We are grateful to H.-H. Tu, A. Shimizu, Y. Chiba, and Z. Wei for useful discussions. The MPS calculations in this work were performed using the ITensor library [64]. YY was supported by the

Special Postdoctoral Researchers Program at RIKEN.

* yasushi.yoneta@riken.jp

- [1] S. Popescu, A. J. Short, and A. Winter, Entanglement and the foundations of statistical mechanics, *Nat. Phys.* **2**, 754 (2006).
- [2] S. Goldstein, J. L. Lebowitz, R. Tumulka, and N. Zanghì, Canonical Typicality, *Phys. Rev. Lett.* **96**, 050403 (2006).
- [3] P. Reimann, Typicality for Generalized Microcanonical Ensembles, *Phys. Rev. Lett.* **99**, 160404 (2007).
- [4] S. Sugiura and A. Shimizu, Thermal Pure Quantum States at Finite Temperature, *Phys. Rev. Lett.* **108**, 240401 (2012).
- [5] S. Sugiura and A. Shimizu, Canonical Thermal Pure Quantum State, *Phys. Rev. Lett.* **111**, 010401 (2013).
- [6] M. Hyuga, S. Sugiura, K. Sakai, and A. Shimizu, Thermal pure quantum states of many-particle systems, *Phys. Rev. B* **90**, 121110(R) (2014).
- [7] K. Goto, Y. Kusuki, K. Tamaoka, and T. Ugajin, Product of random states and spatial (half-)wormholes, *JHEP* **10**, 205.
- [8] K. Okuyama and K. Sakai, Page curve from dynamical branes in JT gravity, *JHEP* **02**, 087.
- [9] K. Okuyama and T. Tachibana, Negativity and its capacity in JT gravity, *JHEP* **02**, 183.
- [10] Z. Wei and Y. Yoneta, Counting atypical black hole microstates from entanglement wedges, *JHEP* **05**, 251.
- [11] Y. Yamaji, T. Suzuki, T. Yamada, S.-i. Suga, N. Kawashima, and M. Imada, Clues and criteria for designing a Kitaev spin liquid revealed by thermal and spin excitations of the honeycomb iridate Na_2IrO_3 , *Phys. Rev. B* **93**, 174425 (2016).
- [12] T. Shimokawa and H. Kawamura, Finite-Temperature Crossover Phenomenon in the $S = 1/2$ Antiferromagnetic Heisenberg Model on the Kagome Lattice, *J. Phys. Soc. Jpn.* **85**, 113702 (2016).
- [13] J. Nasu, Y. Kato, J. Yoshitake, Y. Kamiya, and Y. Motome, Spin-Liquid-to-Spin-Liquid Transition in Kitaev Magnets Driven by Fractionalization, *Phys. Rev. Lett.* **118**, 137203 (2017).
- [14] H. Endo, C. Hotta, and A. Shimizu, From Linear to Non-linear Responses of Thermal Pure Quantum States, *Phys. Rev. Lett.* **121**, 220601 (2018).
- [15] H. Tomishige, J. Nasu, and A. Koga, Interlayer coupling effect on a bilayer Kitaev model, *Phys. Rev. B* **97**, 094403 (2018).
- [16] T. Suzuki and S.-i. Suga, Effective model with strong Kitaev interactions for $\alpha\text{-RuCl}_3$, *Phys. Rev. B* **97**, 134424 (2018).
- [17] J. Oitmaa, A. Koga, and R. R. P. Singh, Incipient and well-developed entropy plateaus in spin- S Kitaev models, *Phys. Rev. B* **98**, 214404 (2018).
- [18] A. Wietek, P. Corboz, S. Wessel, B. Normand, F. Mila, and A. Honecker, Thermodynamic properties of the Shastry-Sutherland model throughout the dimer-product phase, *Phys. Rev. Res.* **1**, 033038 (2019).
- [19] C. Hickey and S. Trebst, Emergence of a field-driven $U(1)$ spin liquid in the Kitaev honeycomb model, *Nat. Commun.* **10**, 530 (2019).
- [20] C. Hickey, C. Berke, P. P. Stavropoulos, H.-Y. Kee, and

S. Trebst, Field-driven gapless spin liquid in the spin-1 Kitaev honeycomb model, *Phys. Rev. Res.* **2**, 023361 (2020).

[21] H. Suzuki, H. Liu, J. Bertinshaw, K. Ueda, H. Kim, S. Laha, D. Weber, Z. Yang, L. Wang, H. Takahashi, K. Fuersich, M. Minola, B. Lotsch, B. Kim, H. Yavaş, M. Daghofer, J. Chaloupka, G. Khaliullin, H. Gretarsson, and B. Keimer, Proximate ferromagnetic state in the Kitaev model material α -RuCl₃, *Nat. Commun.* **12**, 4512 (2021).

[22] H. Shackleton, A. Wietek, A. Georges, and S. Sachdev, Quantum Phase Transition at Nonzero Doping in a Random t -J Model, *Phys. Rev. Lett.* **126**, 136602 (2021).

[23] C. Powers, L. Bassman Oftelie, D. Camps, and W. A. de Jong, Exploring finite temperature properties of materials with quantum computers, *Sci. Rep.* **13**, 1986 (2023).

[24] L. Coopmans, Y. Kikuchi, and M. Benedetti, Predicting Gibbs-State Expectation Values with Pure Thermal Shadows, *PRX Quantum* **4**, 010305 (2023).

[25] Z. Davoudi, N. Mueller, and C. Powers, Towards Quantum Computing Phase Diagrams of Gauge Theories with Thermal Pure Quantum States, *Phys. Rev. Lett.* **131**, 081901 (2023).

[26] Y. O. Nakagawa, M. Watanabe, H. Fujita, and S. Sugiura, Universality in volume-law entanglement of scrambled pure quantum states, *Nat. Commun.* **9**, 1635 (2018).

[27] H. Fujita, Y. O. Nakagawa, S. Sugiura, and M. Watanabe, Page Curves for General Interacting Systems, *JHEP* **12**, 112.

[28] T.-C. Lu and T. Grover, Renyi entropy of chaotic eigenstates, *Phys. Rev. E* **99**, 032111 (2019).

[29] M. Fannes, B. Nachtergaele, and R. F. Werner, Exact Antiferromagnetic Ground States of Quantum Spin Chains, *Europhys. Lett.* **10**, 633 (1989).

[30] M. Fannes, B. Nachtergaele, and R. F. Werner, Valence bond states on quantum spin chains as ground states with spectral gap, *J. Phys. A: Math. Gen.* **24**, L185 (1991).

[31] F. Verstraete and J. I. Cirac, Matrix product states represent ground states faithfully, *Phys. Rev. B* **73**, 094423 (2006).

[32] F. Verstraete, V. Murg, and J. Cirac, Matrix product states, projected entangled pair states, and variational renormalization group methods for quantum spin systems, *Adv. Phys.* **57**, 143 (2008).

[33] U. Schollwöck, The density-matrix renormalization group in the age of matrix product states, *Ann. Phys.* **326**, 96 (2011).

[34] S. R. White, Minimally Entangled Typical Quantum States at Finite Temperature, *Phys. Rev. Lett.* **102**, 190601 (2009).

[35] E. M. Stoudenmire and S. R. White, Minimally entangled typical thermal state algorithms, *New J. Phys.* **12**, 055026 (2010).

[36] S. Garnerone, Pure state thermodynamics with matrix product states, *Phys. Rev. B* **88**, 165140 (2013).

[37] A. Iwaki, A. Shimizu, and C. Hotta, Thermal pure quantum matrix product states recovering a volume law entanglement, *Phys. Rev. Res.* **3**, L022015 (2021).

[38] A. Iwaki and C. Hotta, Thermal pure quantum matrix product states: a simple numerical protocol for finite temperature, *J. Phys.: Conf. Ser.* **2207**, 012031 (2022).

[39] A. Iwaki and C. Hotta, Sample complexity of matrix product states at finite temperature, *Phys. Rev. B* **109**, 224410 (2024).

[40] M. L. Mehta, *Random Matrices*, 3rd ed. (Academic Press, New York, 2004).

[41] Y. Chiba and Y. Yoneta, Exact Thermal Eigenstates of Nonintegrable Spin Chains at Infinite Temperature, *Phys. Rev. Lett.* **133**, 170404 (2024).

[42] For our results, it is sufficient that p satisfies the following conditions: (1) p is the spatial translation on Λ , (2) $p(p(r)) = r$, and (3) the minimum distance between antipodal pairs is $\Theta(N^{1/d})$. It is worth noting that whereas p is unique in one-dimensional systems, it can be chosen in various ways in higher-dimensional systems.

[43] Here, we consider only EAP states that are invariant (up to a phase factor) under spatial translations, as required for subsequent applications.

[44] Interestingly, some EAP states coincide with lattice theory counterparts of crosscap states in (1+1)-dimensional CFTs, studied in the contexts of quantum field theory and mathematical physics [65–70]. However, we consider more general systems beyond (1+1)-dimensional CFTs. Moreover, even when crosscap states can be defined, EAP states generally do not coincide with them. Therefore, to avoid confusion, we refer to $|\text{EAP}(\hat{u})\rangle$ as the EAP state.

[45] If we choose \hat{u} to be the identity operator \hat{I} or one of the Pauli matrices $\hat{\sigma}^\mu(\mu = x, y, z)$, then in each case, $|\Phi(\hat{u})\rangle_{r,p(r)}$ reduces to one of the four Bell states. Thus, Eq. (4) is an extension of the definition of the EAP state presented in Ref. [41].

[46] See Supplemental Material for the derivation.

[47] H. B. Callen, *Thermodynamics and an Introduction to Thermostatistics*, 2nd ed. (John Wiley & Sons, New York, 1985).

[48] F. Verstraete, J. J. García-Ripoll, and J. I. Cirac, Matrix Product Density Operators: Simulation of Finite-Temperature and Dissipative Systems, *Phys. Rev. Lett.* **93**, 207204 (2004).

[49] A. E. Feiguin and S. R. White, Finite-temperature density matrix renormalization using an enlarged Hilbert space, *Phys. Rev. B* **72**, 220401(R) (2005).

[50] E. T. Jaynes, Information theory and statistical mechanics, *Phys. Rev.* **106**, 620 (1957).

[51] E. T. Jaynes, Information theory and statistical mechanics. II, *Phys. Rev.* **108**, 171 (1957).

[52] Z.-Q. Li, L.-P. Yang, Z. Y. Xie, H.-H. Tu, H.-J. Liao, and T. Xiang, Critical properties of the two-dimensional q -state clock model, *Phys. Rev. E* **101**, 060105(R) (2020).

[53] W. Tang, H.-H. Tu, and L. Wang, Continuous Matrix Product Operator Approach to Finite Temperature Quantum States, *Phys. Rev. Lett.* **125**, 170604 (2020).

[54] These boundary terms are necessary to describe a translation-invariant system with periodic boundary conditions on the original lattice. While they are unfavorable for numerical calculations using MPS, they offer the advantage of exponentially suppressing finite-size effects compared to cases where boundary terms are absent and open boundary conditions are imposed [41, 71].

[55] G. Vidal, Efficient Simulation of One-Dimensional Quantum Many-Body Systems, *Phys. Rev. Lett.* **93**, 040502 (2004).

[56] S. R. White and A. E. Feiguin, Real-Time Evolution Using the Density Matrix Renormalization Group, *Phys. Rev. Lett.* **93**, 076401 (2004).

[57] A. J. Daley, C. Kollath, U. Schollwöck, and G. Vidal, Time-dependent density-matrix renormalization-group

using adaptive effective Hilbert spaces, *J. Stat. Mech.* **2004**, P04005 (2004).

[58] E. Lieb, T. Schultz, and D. Mattis, Two soluble models of an antiferromagnetic chain, *Ann. Phys.* **16**, 407 (1961).

[59] Since it is also a real matrix, we can also choose $\hat{u} = \hat{I}$. Both choices yield the same results in the thermodynamic limit.

[60] G. H. Wannier, Antiferromagnetism. The Triangular Ising Net, *Phys. Rev.* **79**, 357 (1950).

[61] Y. Nakata, C. Hirche, C. Morgan, and A. Winter, Unitary 2-designs from random X - and Z -diagonal unitaries, *J. Math. Phys.* **58**, 052203 (2017).

[62] Y. Nakata, D. Zhao, T. Okuda, E. Bannai, Y. Suzuki, S. Tamiya, K. Heya, Z. Yan, K. Zuo, S. Tamate, Y. Tabuchi, and Y. Nakamura, Quantum Circuits for Exact Unitary t -Designs and Applications to Higher-Order Randomized Benchmarking, *PRX Quantum* **2**, 030339 (2021).

[63] D. Poulin, A. Qarry, R. Somma, and F. Verstraete, Quantum Simulation of Time-Dependent Hamiltonians and the Convenient Illusion of Hilbert Space, *Phys. Rev. Lett.* **106**, 170501 (2011).

[64] M. Fishman, S. R. White, and E. M. Stoudenmire, The ITensor Software Library for Tensor Network Calculations, *SciPost Phys. Codebases* **4** (2022).

[65] N. Ishibashi, The Boundary and Crosscap States in Conformal Field Theories, *Mod. Phys. Lett. A* **04**, 251 (1989).

[66] J. Caetano and S. Komatsu, Crosscap States in Integrable Field Theories and Spin Chains, *J. Stat. Phys.* **187**, 30 (2022).

[67] C. Ekman, *Crosscap states in the XXX spin-1/2 spin chain* (2022).

[68] M. Guica and S. F. Ross, Behind the geon horizon, *Class. Quant. Grav.* **32**, 055014 (2015).

[69] A. Maloney and S. F. Ross, Holography on non-orientable surfaces, *Class. Quant. Grav.* **33**, 185006 (2016).

[70] Z. Wei, *Holographic Dual of Crosscap Conformal Field Theory* (2024).

[71] D. Iyer, M. Srednicki, and M. Rigol, Optimization of finite-size errors in finite-temperature calculations of un-ordered phases, *Phys. Rev. E* **91**, 062142 (2015).

[72] H.-H. Tu, Universal Entropy of Conformal Critical Theories on a Klein Bottle, *Phys. Rev. Lett.* **119**, 261603 (2017).

[73] Y. Zhang, A. Hulsch, H.-C. Zhang, W. Tang, L. Wang, and H.-H. Tu, Universal Scaling of Klein Bottle Entropy near Conformal Critical Points, *Phys. Rev. Lett.* **130**, 151602 (2023).

[74] B.-Y. Tan, Y. Zhang, H.-C. Zhang, W. Tang, L. Wang, H.-H. Tu, and Y.-H. Wu, *Extracting the Luttinger parameter from a single wave function* (2024).

[75] M. Binder and T. Barthel, Minimally entangled typical thermal states versus matrix product purifications for the simulation of equilibrium states and time evolution, *Phys. Rev. B* **92**, 125119 (2015).

[76] Z. Wang, P. McClarty, D. Dankova, A. Honecker, and A. Wietek, *Spectroscopy and complex-time correlations using minimally entangled typical thermal states* (2024).

[77] Y. Yoneta, Stationarity of quantum statistical ensembles at first-order phase transition points, *J. Stat. Mech.* **2023**, 093104 (2023).

[78] T. Niemeijer, Some exact calculations on a chain of spins 1/2, *Physica* **36**, 377 (1967).

Supplemental Material for
“Thermal Pure States for Systems with Antiunitary Symmetries
and Their Tensor Network Representations”

DERIVATION OF FORMULAS FOR STATISTICAL-MECHANICAL QUANTITIES

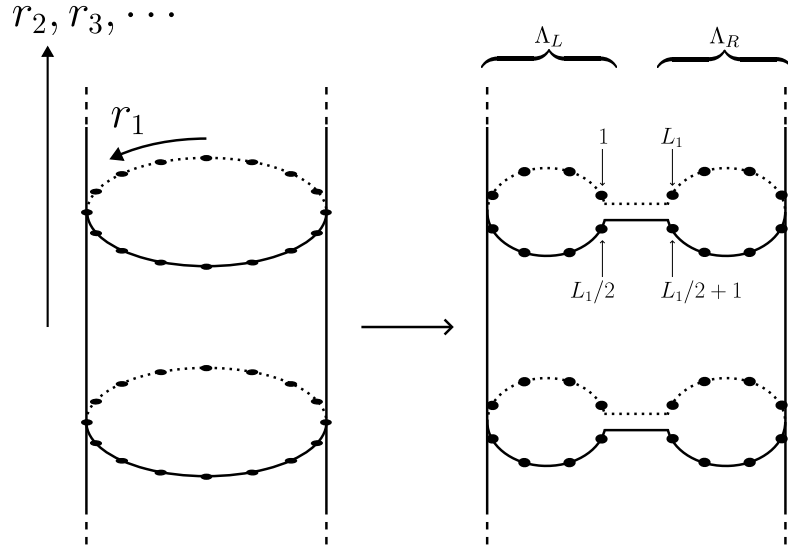
In this supplemental material, we derive formulas for calculating statistical-mechanical quantities from ITE-EAP states under plausible assumptions (shown in Eqs. (S3) and (S4) below).

Truncated imaginary-time evolution

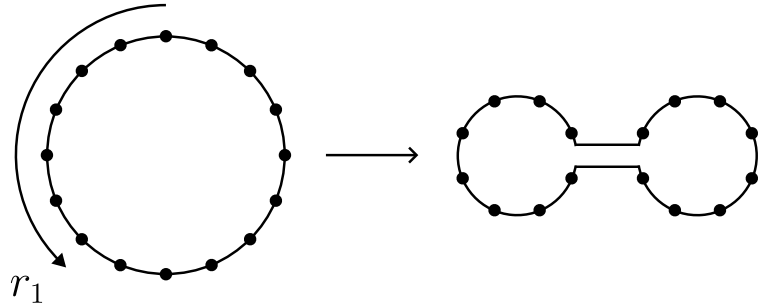
We begin by decomposing the Hamiltonian into three parts: the part that acts only on the “left half” Λ_L , the part that acts only on the “right half” $\Lambda_R = \Lambda \setminus \Lambda_L$, and the interaction between these two subsystems. This decomposition is not unique in general. Here, we consider the following decomposition by defining the interaction \hat{H}_{CT} as a counter term that ensures the equality:

$$\hat{H} = \hat{H}_{N/2} \otimes \hat{I}_R + \hat{I}_L \otimes \hat{H}_{N/2} + \hat{H}_{\text{CT}}. \quad (\text{S1})$$

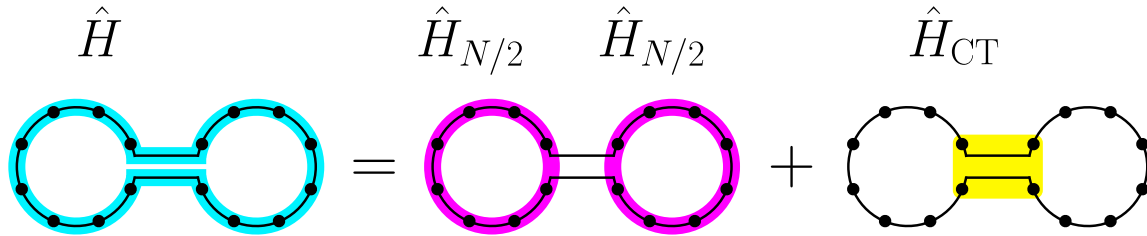
Here, $\hat{H}_{N/2}$ is the Hamiltonian on a lattice $\Lambda_{N/2} = \{1, 2, \dots, L_1/2\} \times \{1, 2, \dots, L_2\} \times \{1, 2, \dots, L_3\} \times \dots \times \{1, 2, \dots, L_d\}$, whose number of lattice sites is $N/2$, with periodic boundary conditions. That is, $\hat{H}_{N/2}$ is the Hamiltonian for the same system as for \hat{H} , except that the side length of the lattice in the first direction is half that of the original lattice. To explain the properties of \hat{H}_{CT} , we virtually deform the lattice by “pinching” the torus so that for all $r_i \in \{1, 2, \dots, L_i\}$ ($i = 2, 3, \dots, d$), lattice points $(1, r_2, r_3, \dots, r_d)$ and $(L_1/2 + 1, r_2, r_3, \dots, r_d)$ are adjacent to $(L_1/2 + 1, r_2, r_3, \dots, r_d)$ and $(L_1, r_2, r_3, \dots, r_d)$, respectively:



For simplicity, we illustrate this by fixing the coordinates of the lattice other than r_1 (r_2, r_3, \dots):

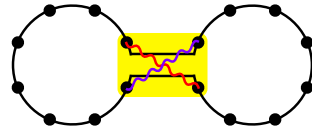


This deformation localizes the boundary between subsystems Λ_L and Λ_R . Consequently, for systems with short-ranged and translation-invariant interactions, the support of each term in Eq. (S1) is as follows:



Thus, \hat{H}_{CT} is an operator supported on a hyperplane of codimension 1 in the deformed lattice (a point for one-dimensional cases and a line for two-dimensional cases), whose volume is negligible compared to the total volume in the thermodynamic limit.

In addition, on the deformed lattice, the entanglement in the EAP state $|\text{EAP}(\hat{u})\rangle$ between a spin near the boundary and its antipodal pair is localized, and $|\text{EAP}(\hat{u})\rangle$ is in a product state with elsewhere:

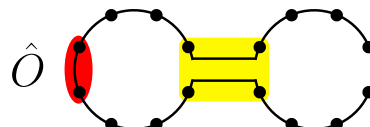


Consequently, in the imaginary-time evolution of $|\text{EAP}(\hat{u})\rangle$, it is anticipated that the presence of \hat{H}_{CT} will not significantly affect the regions far from the boundary between Λ_L and Λ_R , as it does not propagate through correlations in the initial state.

Then we consider the imaginary-time evolution generated by the Hamiltonian without \hat{H}_{CT} and introduce an approximation $|\tilde{\beta}\rangle$ for $|\beta\rangle$ as

$$|\tilde{\beta}\rangle = e^{-\frac{1}{4}\beta[\hat{H} - \hat{H}_{\text{CT}}]} |\text{EAP}(\hat{u})\rangle. \quad (\text{S2})$$

From the above observations, $|\tilde{\beta}\rangle$ is expected to be a good approximation for $|\beta\rangle$. In particular, expectation values in $|\tilde{\beta}\rangle$ of local observables whose supports are far from the boundary between subsystems Λ_L and Λ_R are expected to coincide with those in the ITE-EAP state $|\beta\rangle$ in the thermodynamic limit. Thus, to derive Eq. (9) in the main text, for any local observable \hat{O} with support around $r_1 = L_1/4$, which is $O(L_1)$ distance from the boundary of Λ_L ,



we assume that $|\beta\rangle$ and $|\tilde{\beta}\rangle$ give the same expectation values in the thermodynamic limit:

$$\lim_{N \rightarrow \infty} \frac{\langle \beta | \hat{O} | \beta \rangle}{\langle \beta | \beta \rangle} = \lim_{N \rightarrow \infty} \frac{\langle \tilde{\beta} | \hat{O} | \tilde{\beta} \rangle}{\langle \tilde{\beta} | \tilde{\beta} \rangle}. \quad (\text{S3})$$

Additionally, to derive Eq. (10), we assume that the logarithm of norms of $|\beta\rangle$ and $|\tilde{\beta}\rangle$ coincide in leading order of the thermodynamic limit:

$$\lim_{N \rightarrow \infty} \frac{1}{N} \log \langle \beta | \beta \rangle = \lim_{N \rightarrow \infty} \frac{1}{N} \log \langle \tilde{\beta} | \tilde{\beta} \rangle. \quad (\text{S4})$$

The validity of these assumptions is tested numerically in the main text by verifying formulas (10) and (10) derived from these assumptions.

Properties of $|\tilde{\beta}\rangle$

Let us examine the properties of $|\tilde{\beta}\rangle$ in detail. We write the spin basis of the system on $\Lambda_{N/2}$, i.e., the tensor products of $N/2$ eigenvectors of $\hat{\sigma}^z$, as $|\vec{\sigma}\rangle$. Obviously, $|\vec{\sigma}\rangle$ form the basis for the Hilbert spaces associated with the subsystems on Λ_L and Λ_R . Since the system on Λ is a composite system consisting of two systems on Λ_L and Λ_R , the EAP state $|\text{EAP}(\hat{u})\rangle$ can be expanded using the spin basis as

$$|\text{EAP}(\hat{u})\rangle = \hat{I}_L \otimes \left(\hat{u}^{\otimes N/2} \right) \bigotimes_{r \in \Lambda_L} \left[|0\rangle_r |0\rangle_{p(r)} + |1\rangle_r |1\rangle_{p(r)} \right] = \sum_{\vec{\sigma}} |\vec{\sigma}\rangle_L \otimes \left(\hat{u}^{\otimes N/2} \right) |\vec{\sigma}\rangle_R. \quad (\text{S5})$$

Then, from Eqs. (S1) and (S2), we have

$$\begin{aligned} |\tilde{\beta}\rangle &= \sum_{\vec{\sigma}} e^{-\frac{1}{4}\beta\hat{H}_{N/2}} |\vec{\sigma}\rangle \otimes e^{-\frac{1}{4}\beta\hat{H}_{N/2}} \left(\hat{u}^{\otimes N/2} \right) |\vec{\sigma}\rangle \\ &= \sum_{\vec{\sigma}} e^{-\frac{1}{4}\beta\hat{H}_{N/2}} |\vec{\sigma}\rangle \otimes \left(\hat{u}^{\otimes N/2} \right) \left(\sum_{\vec{\sigma}'} |\vec{\sigma}'\rangle \langle \vec{\sigma}'| \right) \left(\hat{u}^{\otimes N/2} \right)^\dagger e^{-\frac{1}{4}\beta\hat{H}_{N/2}} \left(\hat{u}^{\otimes N/2} \right) |\vec{\sigma}\rangle \\ &= \sum_{\vec{\sigma}, \vec{\sigma}'} e^{-\frac{1}{4}\beta\hat{H}_{N/2}} |\vec{\sigma}\rangle \otimes \langle \vec{\sigma}'| e^{-\frac{1}{4}\beta \left[\left(\hat{u}^{\otimes N/2} \right)^\dagger \hat{H}_{N/2} \left(\hat{u}^{\otimes N/2} \right) \right]} |\vec{\sigma}'\rangle \left(\hat{u}^{\otimes N/2} \right) |\vec{\sigma}'\rangle. \end{aligned} \quad (\text{S6})$$

Since $\hat{H}_{N/2}$ also has symmetry with respect to the antiunitary transformation $\hat{\Theta} = \hat{u}^{\otimes N/2} \hat{K}$, it holds that

$$\langle \vec{\sigma}' | e^{-\frac{1}{4}\beta \left[\left(\hat{u}^{\otimes N/2} \right)^\dagger \hat{H}_{N/2} \left(\hat{u}^{\otimes N/2} \right) \right]} |\vec{\sigma}'\rangle^* = \langle \vec{\sigma}' | e^{-\frac{1}{4}\beta\hat{H}_{N/2}} |\vec{\sigma}'\rangle \quad (\text{S7})$$

for any $|\vec{\sigma}\rangle$ and $|\vec{\sigma}'\rangle$. Therefore, substituting this into Eq. (S6), we get

$$|\tilde{\beta}\rangle = \sum_{\vec{\sigma}, \vec{\sigma}'} e^{-\frac{1}{4}\beta\hat{H}_{N/2}} |\vec{\sigma}\rangle \langle \vec{\sigma}'| e^{-\frac{1}{4}\beta\hat{H}_{N/2}} |\vec{\sigma}'\rangle \otimes \left(\hat{u}^{\otimes N/2} \right) |\vec{\sigma}'\rangle = \sum_{\vec{\sigma}'} e^{-\frac{1}{2}\beta\hat{H}_{N/2}} |\vec{\sigma}'\rangle \otimes \left(\hat{u}^{\otimes N/2} \right) |\vec{\sigma}'\rangle. \quad (\text{S8})$$

Derivation of Eq. (9)

Now, let us derive the formula (9) that gives thermal expectation values of local observables.

Since both $|\beta\rangle$ and $\hat{\rho}_N^{\text{can}}(\beta)$ are translation invariant, without loss of generality, we can assume that \hat{O} has support on Λ_L , particularly around $r_1 = L_1/4$. Thus, we assume Eq. (S3).

On the other hand, from Eq.(S8), for any observable \hat{O} on Λ_L , we have

$$\langle \tilde{\beta} | \hat{O} | \tilde{\beta} \rangle = \text{Tr} \left[e^{-\beta\hat{H}_{N/2}} \hat{O} \right], \quad (\text{S9})$$

$$\langle \tilde{\beta} | \tilde{\beta} \rangle = \text{Tr} \left[e^{-\beta\hat{H}_{N/2}} \right]. \quad (\text{S10})$$

Therefore, we have

$$\frac{\langle \tilde{\beta} | \hat{O} | \tilde{\beta} \rangle}{\langle \tilde{\beta} | \tilde{\beta} \rangle} = \text{Tr} \left[\hat{\rho}_{N/2}^{\text{can}}(\beta) \hat{O} \right], \quad (\text{S11})$$

where $\hat{\rho}_{N/2}^{\text{can}}(\beta) \propto e^{-\beta \hat{H}_{N/2}}$ is the Gibbs state for $\hat{H}_{N/2}$. Combining this with assumption (S3), in the thermodynamic limit, we obtain

$$\lim_{N \rightarrow \infty} \frac{\langle \beta | \hat{O} | \beta \rangle}{\langle \beta | \beta \rangle} = \lim_{N \rightarrow \infty} \text{Tr} \left[\hat{\rho}_N^{\text{can}}(\beta) \hat{O} \right]. \quad (\text{S12})$$

Therefore, we have Eq. (9).

Derivation of Eq. (10)

Finally, let us derive the formula (10) for the free energy density. From Eq. (S10), we immediately get

$$\frac{2}{N} \log \langle \tilde{\beta} | \tilde{\beta} \rangle = \frac{1}{N/2} \log Z_{N/2}, \quad (\text{S13})$$

where $Z_{N/2} = \text{Tr} \left[e^{-\beta \hat{H}_{N/2}} \right]$ is the partition function for the system with Hamiltonian $\hat{H}_{N/2}$. Hence the thermodynamic limit yields

$$\lim_{N \rightarrow \infty} \frac{2}{N} \log \langle \tilde{\beta} | \tilde{\beta} \rangle = -\beta f(\beta) \quad (\text{S14})$$

Therefore, combining this with assumption (S4), we obtain

$$\lim_{N \rightarrow \infty} \frac{2}{N} \log \langle \beta | \beta \rangle = -\beta f(\beta). \quad (\text{S15})$$

Therefore, we have Eq. (10).

It is worth mentioning that this is consistent with the results of field theoretical analysis for $(1+1)$ -dimensional CFTs, where EAP states correspond to crosscap states. Consider a (perturbed) CFT defined on a spatial circle of circumference L . According to the results of Refs. [72–74], the cylinder partition function with crosscap boundary states,

$$Z^C(L, \beta/2) = \langle \text{EAP}(\hat{u}) | e^{-\frac{1}{2}\beta \hat{H}} | \text{EAP}(\hat{u}) \rangle (= \langle \beta | \beta \rangle), \quad (\text{S16})$$

coincides with the partition function $Z^K(L/2, \beta)$ on the Klein bottle, a rectangular $[0, L/2] \times [0, \beta]$ with sides identified by the relations $(x, 0) \sim (x, \beta)$ for $0 \leq x \leq L/2$ and $(0, \tau) \sim (L/2, \beta - \tau)$ for $0 \leq \tau \leq \beta$,

$$Z^C(L, \beta/2) = Z^K(L/2, \beta). \quad (\text{S17})$$

Furthermore, the ratio between $Z^K(L/2, \beta)$ and the partition function $Z^T(L/2, \beta)$ on the torus, which is the usual partition function $Z_{L/2}$ for a system of length $L/2$ at the inverse temperature β , approaches a constant independent of L in the thermodynamic limit,

$$\frac{Z^K(L/2, \beta)}{Z^T(L/2, \beta)} = O(L^0). \quad (\text{S18})$$

Therefore, we have

$$\lim_{L \rightarrow \infty} \frac{2}{L} \log \langle \beta | \beta \rangle = \lim_{L \rightarrow \infty} \frac{1}{L/2} \log Z_{L/2}. \quad (\text{S19})$$

This is the field-theoretic counterpart of Eq. (10). Our claim in this subsection is that this holds in general, not just for $(1+1)$ -dimensional CFT systems.

DYNAMICAL ITE-EAP STATE ALGORITHM

The ITE-EAP state can also correctly describe dynamics starting from an equilibrium state. However, as time evolves, the ITE-EAP state loses its simple entanglement structure, making it hard to represent efficiently as a tensor network state and challenging to compute efficiently over long timescales. To clarify this, let us consider the example of calculating a time-dependent correlation function. The time-dependent correlation function of local observables \hat{A} and \hat{B} is defined as

$$C(t) = \lim_{N \rightarrow \infty} \text{Tr} \left[\hat{\rho}_N^{\text{can}}(\beta) \hat{A}(t) \hat{B} \right], \quad (\text{S20})$$

where $\hat{A}(t) = e^{+i\hat{H}t} \hat{A} e^{-i\hat{H}t}$ is the Heisenberg operator for \hat{A} . Such time-dependent quantities can also be computed from the ITE-EAP state in a manner analogous to the algorithm developed for the METTS method [75, 76].

In systems with short-range interactions, the Heisenberg operator for a local observable with t independent of N can be well approximated as a local observable [77]. Consequently, in the same manner as for Eq. (9), we can show that for $t \in \mathbb{R}$ independent of N , the following holds:

$$C(t) = \lim_{N \rightarrow \infty} \frac{\langle \beta | \hat{A}(t) \hat{B} | \beta \rangle}{\langle \beta | \beta \rangle}. \quad (\text{S21})$$

To numerically calculate the right-hand side of the above equation, we proceed as follows. First, construct the ITE-EAP state $|\beta\rangle$ using the algorithm described in the main text. With this $|\beta\rangle$, set

$$|\varphi_1(0)\rangle = \frac{1}{\sqrt{\langle \beta | \beta \rangle}} \hat{B} |\beta\rangle, \quad |\varphi_2(0)\rangle = \frac{1}{\sqrt{\langle \beta | \beta \rangle}} |\beta\rangle. \quad (\text{S22})$$

Next, evolve these states forward in time as

$$|\varphi_1(t)\rangle = e^{i\hat{H}t} |\varphi_1(0)\rangle, \quad |\varphi_2(t)\rangle = e^{i\hat{H}t} |\varphi_2(0)\rangle. \quad (\text{S23})$$

Finally, compute the product $\langle \varphi_2(t) | \hat{A} | \varphi_1(t) \rangle$. Then, since

$$\langle \varphi_2(t) | \hat{A} | \varphi_1(t) \rangle = \frac{\langle \beta | \hat{A}(t) \hat{B} | \beta \rangle}{\langle \beta | \beta \rangle}, \quad (\text{S24})$$

the time-dependent correlation function $C(t)$ can be computed as

$$C(t) = \lim_{N \rightarrow \infty} \langle \varphi_2(t) | \hat{A} | \varphi_1(t) \rangle. \quad (\text{S25})$$

As explained in the main text, by rearranging the lattice, $|\beta\rangle$ can be transformed into a state with low entanglement. Furthermore, on the rearranged lattice, \hat{H} retains short-range interactions. Therefore, for short timescales, both $|\varphi_1(t)\rangle$ and $|\varphi_2(t)\rangle$ exhibit low entanglement and can be efficiently represented as tensor network states. However, as time evolves, the ITE-EAP state is expected to develop a more intricate entanglement structure, making it increasingly difficult to express as a tensor network state (see the example below).

As a demonstration, we apply the algorithm explained above to the one-dimensional XY model (defined by Eq. (13)) with $N = 100$ and compute the time-dependent correlation function of the Pauli matrix $\hat{\sigma}_1^z$,

$$C(t) = \lim_{N \rightarrow \infty} \text{Tr} \left[\hat{\rho}_N^{\text{can}}(\beta) \hat{\sigma}_1^z(t) \hat{\sigma}_1^z \right]. \quad (\text{S26})$$

In Fig. S1a, we plot the time-dependent correlation function $C(t)$ computed from the ITE-EAP state. The numerical results show close agreement with the exact solution [78], with only slight deviations. These small discrepancies arise from using a relatively large truncation threshold of 10^{-6} to reduce computational costs. However, as illustrated in Fig. S1b, the bipartite entanglement of the time evolved ITE-EAP state $|\varphi_2(t)\rangle$ on the rearranged lattice (ladder) grows with time, resulting in an increase in the bond dimension of the MPS. This severely degrades computational efficiency. Thus, while the ITE-EAP state correctly provides dynamical properties, it is practically challenging to perform numerical simulations over long timescales.

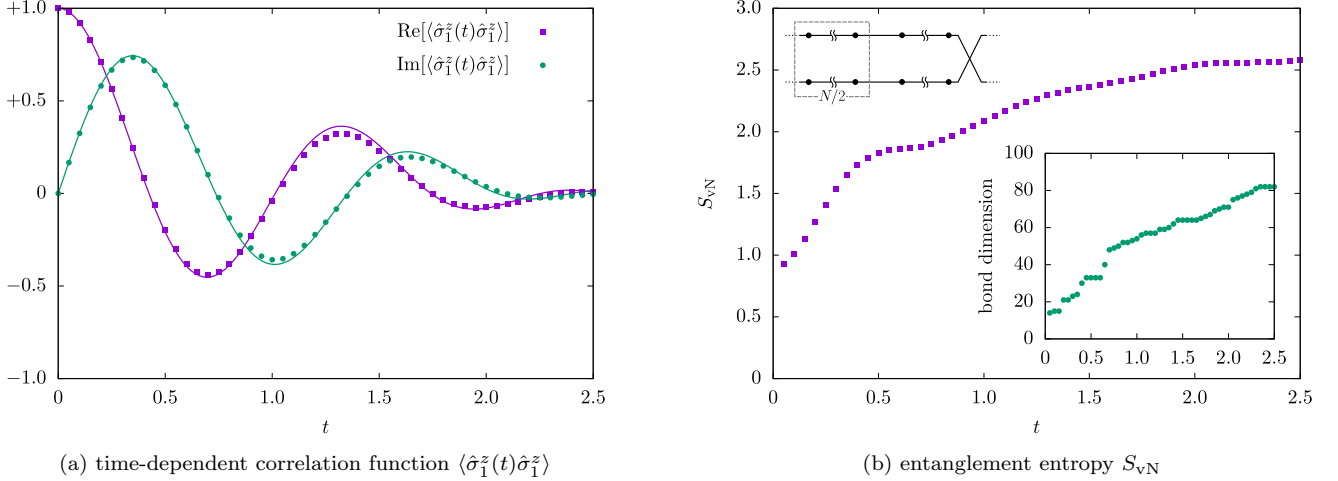


FIG. S1. Dynamical properties of the ITE-EAP state for the one-dimensional XY model with $J^{xx} = 1$, $J^{yy} = 1/2$ and $N = 100$. (a) Time-dependent correlation function $\langle \hat{\sigma}_1^z(t) \hat{\sigma}_1^z \rangle$ at the inverse temperature $\beta = 1$. The solid line represents the exact solution in the thermodynamic limit. (b) Entanglement entropy of the time evolved ITE-EAP state $|\varphi_2(t)\rangle$ at the inverse temperature $\beta = 1$ for a center cut of the ladder. The inset shows the bond dimension of the MPS at the center cut. Real and Imaginary-time evolution are carried out using a second-order Trotter decomposition with a time step of 0.05. We set a truncation threshold of 10^{-6} .